# Evolution of polarization and space charges in semiconducting ferroelectrics

Phanish Suryanarayana and Kaushik Bhattacharya

## Related Articles

High-temperature ferroelectric behaviors of poly(vinylidene fluoride-trifluoroethylene) copolymer ultrathin films with electroactive interlayers
J. Appl. Phys. 111, 064506 (2012)

The influence of Mn substitution on the local structure of Na0.5Bi0.5TiO3 crystals: Increased ferroelectric ordering and coexisting octahedral tilts
J. Appl. Phys. 111, 064109 (2012)

The improved polarization retention through high-field charge injection in highly strained BiFeO3 thin films with preferred domain orientations
Appl. Phys. Lett. 100, 132901 (2012)

Structural phase transitions in Ti-doped Bi1-xNdxFeO3 ceramics
J. Appl. Phys. 111, 064107 (2012)

Ferroelectric domain structures of 0.4-µm-thick Pb(Zr,Ti)O3 films prepared by polyvinylpyrrolidone-assisted Sol-Gel method
J. Appl. Phys. 111, 054109 (2012)

## Additional information on J. Appl. Phys.

Journal Homepage: http://jap.aip.org/

Journal Information: http://jap.aip.org/about/about_the_journal

Top downloads: http://jap.aip.org/features/most_downloaded

Information for Authors: http://jap.aip.org/authors

# Evolution of polarization and space charges in semiconducting ferroelectrics

Phanish Suryanarayana and Kaushik Bhattacharya[a)]
*Division of Engineering and Applied Science, California Institute of Technology, Pasadena,
California 91125, USA*

Ferroelectric perovskites and polymers that are used in a variety of electronic, ultrasonic, and optical applications are often wide-band-gap semiconductors. We present a time-dependent and thermodynamically consistent theory that describes the evolution of polarization and space charges in such materials. We then use it to show that the semiconducting nature of ferroelectrics can have a profound effect on polarization domain switching, hysteresis, and leakage currents. Further, we show how hysteresis and leakage are affected by doping, film thickness, electrode work function, ambient temperature, and loading frequency. © *2012 American Institute of Physics*. [doi:10.1063/1.3678598]

## I. INTRODUCTION

Ferroelectric perovskites are paraelectric (non-polar) above the Curie temperature, but become spontaneously polarized below it, due to a loss of centrosymmetry.[1] The spontaneous polarization is often accompanied by a mechanical distortion. The anisotropy introduced by the polarization enables birefringences, and the loss of centrosymmetry enables piezoelectricity. The soft modes of the phase transitions give rise to large dielectric constants, and the loss of symmetry enables domain switching between domains of symmetry-related polarizations. All of these endow the material with fascinating properties that enable applications, including optical modulators, non-volatile memories, capacitors, sensors, actuators, and holographic storage media.[2–6]

The range of phenomena, properties, and applications have motivated a number of models of these materials going back to the pioneering work of Devonshire,[7,8] as reviewed before.[4,9] Phase-field and other coarse-grained models which describe behavior at the domain and larger scales almost always assume that the ferroelectric is an insulator. However, a vast majority of the perovskite and polymer ferroelectrics are, in fact, wide-band-gap semiconductors. Since ferroelectrics are often used with metal electrodes, we can expect the formation of depletion layers near the metal-ferroelectric interface, development of a built-in potential, and associated band bending. This, in turn, has a significant impact on the ferroelectric properties and performance as observed by the dependence of the fatigue life and dielectric breakdown on the choice of electrodes.[10–12] Further, it has been noticed that defects often decorate domain walls[13,14] and that domain patterns can be manipulated using light via the generation of photoelectrons,[3] highlighting the semiconducting nature of the ferroelectric.

This has motivated some efforts at incorporating the semiconducting properties of the ferroelectric, by making phenomenological assumptions about either the profile of

polarization[15–19] or free charges.[20–22] Recently, Xiao *et al.*[23–25] have proposed a model that comprehensively treats semiconducting ferroelectrics with no *a priori* assumption on either the space charge or polarization. However, these are limited to equilibrium profiles. On the other hand, time-dependent models based on the Landau-Khalatnikov equation have been developed by Morozovska *et al.*[26–29] Even so, these models are restricted to volume averaged values of quantities and not their spatial variation.

In this paper, we build on the prior work to develop a time-dependent and thermodynamically consistent theory that describes the evolution of the space charge and polarization in semiconducting ferroelectrics. Specifically, we develop thermodynamically consistent kinetic equations that describe the evolution of space-charges and polarization domains when subjected to a time-varying applied field. Further, we carefully incorporate band-bending and other subtle effects at the metal-ferroelectric interface.

The remainder of the paper is arranged as follows. First, we provide a detailed description of the formulation in Sec. II. Next, we describe the numerical implementation and validate it through a number of test cases in Sec. III. Finally, we conclude in Sec. IV.

## II. THEORY AND FORMULATION

### A. Setup

Consider the metal-ferroelectric-metal (MFM) configuration in Fig. 1, where the ferroelectric occupies a region $\Omega$ with boundary $\partial\Omega$ and outward normal $\hat{\mathbf{m}}$. The metal electrodes are denoted by $C_1$, $C_2$ with boundaries $\partial C_1$, $\partial C_2$ and work functions $\Phi_1$, $\Phi_2$, respectively. Let $\partial\Omega \cap \partial C_1 = S_1$ and $\partial\Omega \cap \partial C_2 = S_2$. The circuit is completed by connecting the electrodes to the terminals of a battery, maintaining a time-varying potential difference of $V(t)$ across the MFM system. We assume, for definiteness, that the dominant impurities in the ferroelectric are single electron donors and that there are no surface states, but note that these can be easily relaxed. We neglect the deformation and treat the ferroelectric as rigid. Small deformations can be incorporated easily, but finite
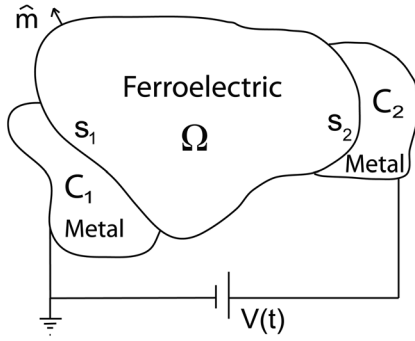
FIG. 1.  Schematic situation.

deformations require special care.[24] We assume that all the processes are isothermal with temperature as a parameter.

### B. Electrostatics and conservation laws

The charge density $\rho$, electrostatic potential $\phi$, and polarization **p** are related through Maxwell's equation

$$\nabla \cdot (-\varepsilon_0 \nabla \phi + \mathbf{p}\chi_\Omega) = \rho\chi_\Omega, \tag{1}$$

where $\chi_\Omega$ is the characteristic function

$$\chi_\Omega(\mathbf{x}) = \begin{cases} 1, & \text{if } \mathbf{x} \in \Omega \\ 0, & \text{otherwise.} \end{cases} \tag{2}$$

The charge density can be represented by

$$\rho = q(N_d^+ - n_c + p_v), \tag{3}$$

where $q$ is the magnitude of the charge of an electron, $N_d^+$ is the number of ionized donors, and $n_c$ and $p_v$ are the number of electrons and holes in the conduction and valence bands, respectively. We can write the following conservation laws:

$$\begin{aligned} \dot{n}_c &= -\nabla \cdot \mathbf{J}_{n_c} + \xi_{cd} + \xi_{cv}, \\ \dot{p}_v &= -\nabla \cdot \mathbf{J}_{p_v} + \xi_{cv} + \xi_{dv}, \\ \dot{N}_d^0 &= -\nabla \cdot \mathbf{J}_{N_d^0} - \xi_{cd} + \xi_{dv}, \\ \dot{N}_d^+ &= -\nabla \cdot \mathbf{J}_{N_d^+} + \xi_{cd} - \xi_{dv}, \end{aligned} \tag{4}$$

where $N_d^0$ is the number of non-ionized donors, **J** denotes the flux of the respective subscripted quantity, and the overdot represents the time derivative. Further, $\xi_{cd}$, $\xi_{cv}$, and $\xi_{dv}$ represent the inter-band electron evolution, as depicted in Fig. 2. Note that we have made the "effective density of states" approximation for the conduction and valence bands.

### C. Potential energy of the system
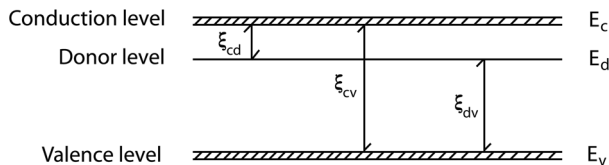
The total potential energy of the system can be written as



FIG. 2.  Inter-band electron evolution.

$$\mathcal{P} = \int_\Omega W \, dV + \frac{\varepsilon_0}{2} \int_{\mathbb{R}^3} |\nabla \phi|^2 \, dV - V \int_{\partial C_2} \sigma \, dS, \tag{5}$$

where $\sigma$ is the charge density on the surface of $C_2$. Above, the first term represents the free or stored energy in the ferroelectric, the second term corresponds to the electrostatic energy in all of space, and the third term is the work done by the battery in maintaining the applied potential. We postulate the following additive form for the free energy density of the ferroelectric:

$$\begin{aligned} W = W_p(\mathbf{p}) + W_g(\nabla \mathbf{p}) + W_{n_c}(n_c) + W_{p_v}(p_v) \\ + W_{N_d}(N_d^0, N_d^+). \end{aligned} \tag{6}$$

Note that temperature is a parameter in each of these terms. $W_p(\mathbf{p})$ is the classical Devonshire[7,8] energy that depends on polarization density **p** and has a multi-well structure below the Curie temperature that corresponds to multiple (symmetry-related) spontaneous polarizations. We set $W_g(\nabla \mathbf{p}) = \frac{1}{2}k|\nabla \mathbf{p}|^2$ to be the gradient or exchange energy that penalizes rapid changes in polarization and is critical in determining the domain wall structure. The remaining terms correspond to the free energy of electrons in the conduction band, holes in the valence band, and donors. Treating each of these systems as a microcanonical ensemble, we obtain the partition functions,

$$\begin{aligned} \mathcal{Z}_{n_c} &= \frac{N!}{n_c!(N-n_c)!}e^{-\beta n_c E_c}, \\ \mathcal{Z}_{p_v} &= \frac{P!}{p_v!(P-p_v)!}e^{-\beta(P-p_v)E_v}, \\ \mathcal{Z}_{N_d} &= \frac{(N_d^0 + N_d^+)!}{N_d^0!N_d^+!}2^{N_d^0}e^{-\beta E_d N_d^0}, \end{aligned} \tag{7}$$

where $N$ and $P$ are the "effective density of states" in the conduction and valence bands, respectively. Also, $\beta = \frac{1}{k_B T}$, where $k_B$ is the Boltzmann's constant and $T$ is the temperature. Using standard relations,

$$\begin{aligned} W_{n_c}(n_c) &= n_c E_c - \frac{1}{\beta}\Big[N \log N - n_c \log n_c - (N - n_c) \\ &\quad \times \log(N - n_c)\Big], \\ W_{p_v}(p_v) &= (P - p_v)E_v - \frac{1}{\beta}\Big[P \log P - p_v \log p_v - (P - p_v) \\ &\quad \times \log(P - p_v)\Big], \\ W_{N_d}(N_d^0, N_d^+) &= E_d N_d^0 - \frac{1}{\beta}\Big[N_d \log N_d \\ &\quad - N_d^0 \log N_d^0 - N_d^+ \log N_d^+ + N_d^0 \log 2\Big]. \end{aligned} \tag{8}$$

### D. Driving forces and electro-chemical potentials

We seek to find the thermodynamic driving force driving the evolution of the polarization and the electro-chemical potentials driving the evolution of the space charges. One approach is to study the variation of the total potential energy in Eq. (5) with respect to the polarization and the space charges. We obtain, after a lengthy, but relatively straightforward calculation using the divergence theorem that

$$\delta \mathcal{P} = \int_\Omega \left\{ \left( \nabla \cdot \left( \frac{\partial W}{\partial \nabla \mathbf{p}} \right) - \frac{\partial W}{\partial \mathbf{p}} - \nabla \phi \right) \cdot \delta \mathbf{p} \right.$$
$$+ \left( \frac{\partial W}{\partial n_c} - q\phi \right) \delta n_c + \left( \frac{\partial W}{\partial p_v} + q\phi \right) \delta p_v + \frac{\partial W}{\partial N_d^0} \delta N_d^0$$
$$\left. + \left( \frac{\partial W}{\partial N_d^+} + q\phi \right) \delta N_d^+ \right\} dV + \int_{\partial \Omega} \left( \frac{\partial W}{\partial \nabla \mathbf{p}} \hat{\mathbf{m}} \right) \cdot \delta \mathbf{p} \; dS. \tag{9}$$

We set the driving force and the electro-chemical potentials to be the quantities that are conjugate to the variations. Thus, the driving force governing the evolution of the polarization is

$$\mathbf{d_p} = \nabla \cdot \left( \frac{\partial W}{\partial \nabla \mathbf{p}} \right) - \frac{\partial W}{\partial \mathbf{p}} - \nabla \phi, \tag{10}$$

and the electro-chemical potentials are

$$\mu_{n_c} = \frac{\partial W}{\partial n_c} - q\phi, \quad \mu_{p_v} = \frac{\partial W}{\partial p_v} + q\phi,$$
$$\mu_{N_d^0} = \frac{\partial W}{\partial N_d^0}, \quad \mu_{N_d^+} = \frac{\partial W}{\partial N_d^+} + q\phi. \tag{11}$$

For future use, we substitute Eq. (8) into Eq. (11) and solve for the space charges in terms of the electro-chemical potentials. We recover the Fermi-Dirac distribution for fermions,

$$n_c = \frac{N}{1 + e^{\beta(E_c - q\phi - \mu_{n_c})}}, \quad p_v = \frac{P}{1 + e^{\beta(-E_v + q\phi - \mu_{p_v})}},$$
$$N_d^+ = N_d \left( 1 - \frac{1}{1 + \frac{1}{2} e^{\beta(E_d - q\phi - (\mu_{N_d^0} - \mu_{N_d^+}))}} \right). \tag{12}$$

### E. Inter-band electron evolution

We model the inter-band electron evolution as the following reversible reactions:

$$N_d^+ + e^- \underset{k_1}{\overset{k_{1f}}{\rightleftarrows}} N_d^0, \quad e^- + h \underset{k_2}{\overset{k_{2f}}{\rightleftarrows}} 0, \quad N_d^0 + h \underset{k_3}{\overset{k_{3f}}{\rightleftarrows}} N_d^+. \tag{13}$$

Therefore,

$$\xi_{cd} = k_1 N_d^0 - k_{1f} N_d^+ n_c, \quad \xi_{cv} = k_2 P - k_{2f} n_c p_v,$$
$$\xi_{dv} = k_3 N_d^+ - k_{3f} N_d^0 p_v. \tag{14}$$

We substitute for the space charges from Eq. (12), and, in order to obtain explicit expressions for the inter-band electron evolution, we assume $n_c \ll N$ and $p_v \ll P$. Now, at equilibrium, $\mu_{n_c} = -\mu_{p_v} = \mu_{N_d^0} - \mu_{N_d^+}$ and $\xi_{cd} = \xi_{cv} = \xi_{dv} = 0$. We use this to obtain relations between the backward and forward rate constants for each reaction. Putting all these together,

$$\xi_{cd} = k_1 N_d^0 \left( 1 - e^{\beta(\mu_{n_c} + \mu_{N_d^+} - \mu_{N_d^0})} \right), \; \xi_{cv} = k_2 P \left( 1 - e^{\beta(\mu_{n_c} + \mu_{p_v})} \right),$$
$$\xi_{dv} = k_3 N_d^+ \left( 1 - e^{\beta(\mu_{p_v} + \mu_{N_d^0} - \mu_{N_d^+})} \right). \tag{15}$$

### F. Flux

The flux of space charges is proportional to the gradient to the electro-chemical potentials,

$$\mathbf{J_{n_c}} = -\mathbf{K_1} \nabla \mu_{n_c}, \quad \mathbf{J_{p_v}} = -\mathbf{K_2} \nabla \mu_{p_v},$$
$$\mathbf{J_{N_d^0}} = -\mathbf{K_3} \nabla \mu_{N_d^0}, \quad \mathbf{J_{N_d^+}} = -\mathbf{K_4} \nabla \mu_{N_d^+}, \tag{16}$$

with diffusion coefficients $\mathbf{K_1}$, $\mathbf{K_2}$, $\mathbf{K_3}$, and $\mathbf{K_4}$.

### G. Boundary conditions

The flux of donors and holes through any interface is negligible. Therefore, we set $\mathbf{J_{p_v}} \cdot \hat{\mathbf{m}} = \mathbf{J_{N_d^0}} \cdot \hat{\mathbf{m}} = \mathbf{J_{N_d^+}} \cdot \hat{\mathbf{m}} = 0$ on $\partial\Omega$. Similarly, we have no flux of electrons in the free regions of the ferroelectric, $\mathbf{J_{n_c}} \cdot \hat{\mathbf{m}} = 0$ on $\partial\Omega \backslash (S_1 \cup S_2)$. This leaves the electron transport through the metal-ferroelectric interface $S_1 \cup S_2$. We proceed as before with an "effective density of states" approximation and model the flux of electrons through the metal-ferroelectric interface as a reversible reaction between the electrons in the metal and positions in the conduction band,

$$e_m^- + pos \underset{k_b}{\overset{k_f}{\rightleftarrows}} e_s^-, \tag{17}$$

where $e_m^-$ and $e_s^-$ represent the electrons in the metal and conduction band of the ferroelectric, respectively, and $pos$ refers to the positions available in the conduction band of the ferroelectric. We can obtain the dependence of these quantities on the metal potential $\hat{\phi}$ and work function $\Phi = -E_{fm}$, as in Sec. II E,

$$[e_m^-] = N_c^m e^{-\beta(\xi^m - (E_{fm} - q\hat{\phi}))}, \; [pos] = N,$$
$$[e_s^-] = N e^{-\beta(E_c - \mu_{n_c} - q\hat{\phi})}, \tag{18}$$

where $\xi^m$ represents the energy of $e_m^-$. By balancing the forward and backward rates $k_b$ and $k_f$ at equal electro-chemical potential, as in Sec. II E, we obtain

$$\mathbf{J_{n_c}} \cdot \hat{\mathbf{m}} = k_b N e^{\beta(E_{fm} - E_c)} \left( e^{\beta(\mu_{n_c} - E_{fm} + q\hat{\phi})} - 1 \right) \quad \text{on } S_1 \cup S_2, \tag{19}$$

where $\hat{\phi}$ and $E_{fm}$ are appropriately chosen for $C_1$ and $C_2$. This is consistent with established relations for current through a metal-semiconductor junction.[30,31]

### H. Polarization evolution

We postulate that the polarization evolves proportional to its driving force (Eq. (10)), so that

$$\eta \dot{\mathbf{p}} = \nabla \cdot \left( \frac{\partial W}{\partial \nabla \mathbf{p}} \right) - \frac{\partial W}{\partial \mathbf{p}} - \nabla \phi, \tag{20}$$

subject to the natural boundary condition $\left( \frac{\partial W}{\partial \nabla \mathbf{p}} \right) \hat{\mathbf{m}} = 0$. Above, $\eta$ is an inverse mobility.

### I. Final equations

We collect the final equations along with the corresponding boundary conditions. The polarization evolves as

$$\eta \dot{\mathbf{p}} = \nabla \cdot \left( \frac{\partial W}{\partial \nabla \mathbf{p}} \right) - \frac{\partial W}{\partial \mathbf{p}} - \nabla \phi \ \text{ in } \ \Omega,$$
$$\left( \frac{\partial W}{\partial \nabla \mathbf{p}} \right) \hat{\mathbf{m}} = 0 \ \text{ on } \ \partial \Omega. \tag{21}$$

The electrostatic potential is determined by

$$\nabla \cdot (-\varepsilon_0 \nabla \phi + \mathbf{p} \chi_\Omega) = \rho \chi_\Omega \ \text{ in } \ \mathbb{R}^3 \backslash C_1 \cup C_2,$$
$$\phi = 0 \text{ on } S_1, \ \phi = V \text{ on } S_2 \text{ and } \phi \to 0 \text{ as } |x| \to \infty. \tag{22}$$

The space-charge transport and evolution are given by

$$\dot{n}_c = \nabla \cdot (\mathbf{K_1} \nabla \mu_{n_c}) + k_1 N_d^0 \left( 1 - e^{\beta(\mu_{n_c} + \mu_{N_d^+} - \mu_{N_d^0})} \right)$$
$$+ k_2 P \left( 1 - e^{\beta(\mu_{n_c} + \mu_{p_v})} \right) \ \text{ in } \ \Omega,$$
$$\dot{p}_v = \nabla \cdot (\mathbf{K_2} \nabla \mu_{p_v}) + k_2 P \left( 1 - e^{\beta(\mu_{n_c} + \mu_{p_v})} \right)$$
$$+ k_3 N_d^+ \left( 1 - e^{\beta(\mu_{p_v} + \mu_{N_d^0} - \mu_{N_d^+})} \right) \ \text{ in } \ \Omega,$$
$$\dot{N}_d^0 = \nabla \cdot (\mathbf{K_3} \nabla \mu_{N_d^0}) - k_1 N_d^0 \left( 1 - e^{\beta(\mu_{n_c} + \mu_{N_d^+} - \mu_{N_d^0})} \right) \tag{23}$$
$$+ k_3 N_d^+ \left( 1 - e^{\beta(\mu_{p_v} + \mu_{N_d^0} - \mu_{N_d^+})} \right) \ \text{ in } \ \Omega,$$
$$\dot{N}_d^+ = \nabla \cdot (\mathbf{K_4} \nabla \mu_{N_d^+}) + k_1 N_d^0 \left( 1 - e^{\beta(\mu_{n_c} + \mu_{N_d^+} - \mu_{N_d^0})} \right)$$
$$- k_3 N_d^+ \left( 1 - e^{\beta(\mu_{p_v} + \mu_{N_d^0} - \mu_{N_d^+})} \right) \ \text{ in } \ \Omega,$$

with the corresponding boundary conditions

$$\mathbf{J_{n_c}} \cdot \hat{\mathbf{m}} = k_4 \left( e^{\beta(\mu_{n_c} + \Phi_1)} - 1 \right) \text{ on } \ S_1,$$
$$\mathbf{J_{n_c}} \cdot \hat{\mathbf{m}} = k_5 \left( e^{\beta(\mu_{n_c} + \Phi_2 + qV)} - 1 \right) \text{ on } \ S_2,$$
$$\mathbf{J_{n_c}} \cdot \hat{\mathbf{m}} = 0 \ \text{ on } \ \partial\Omega \backslash S_1 \cup S_2, \tag{24}$$
$$\mathbf{J_{p_v}} \cdot \hat{\mathbf{m}} = 0 \ \text{ on } \ \partial\Omega, \quad \mathbf{J_{N_d^0}} \cdot \hat{\mathbf{m}} = 0 \ \text{ on } \ \partial\Omega,$$
$$\mathbf{J_{N_d^+}} \cdot \hat{\mathbf{m}} = 0 \ \text{ on } \ \partial\Omega,$$

where the electro-chemical potentials $\mu$ are given by Eq. (11) and fluxes $\mathbf{J}$ are given by Eq. (16). In Appendix A, we show that this model is indeed thermodynamically consistent.

## III. NUMERICAL IMPLEMENTATION AND CASE STUDIES

We now apply the theory developed in the previous section to a one-dimensional situation, as appropriate for a thin film with top and bottom electrodes. We use a second order, implicit finite-difference scheme to discretize the equations and solve them using the Newton trust-region dogleg method.[32] We start with a uniform profile and study the response of n-doped barium titanate to an applied voltage.

The Devonshire energy for barium titanate in one dimension is given by

$$W_p(p) = a(T - T_0)p^2 + b_0(T - T_1)p^4 + cp^6. \tag{25}$$

The material parameters and constants in this energy, as well as those introduced earlier, are listed in Table I. They follow earlier works.[1,24] Since the exact values of some of the material parameters are unknown and only their relative magnitudes are of any significance in our calculations, we indicate their values with a dimensionless constant $\alpha$. (We have verified that the behavior we report is robust and does not qualitatively change with variation of these parameters.) We take $K_3 = K_4 = 0$, since the mobility of the donors is extremely low; we also take $\eta = 0$, so that we can focus on the space-charge evolution. Unless stated otherwise, the temperature is taken to be 300 K and the work function of the metal electrodes is $\Phi_1 = \Phi_2 = \Phi = 5.3$ eV. Typical values of doping concentration in barium titanate ranges from 10 to 1000 ppm,[24] corresponding to $N_d = 10^{24}$–$10^{26}$ m$^{-3}$. In this work, we will restrict ourselves to the range $N_d = 10^{24}$–$10^{25}$ m$^{-3}$. Higher doping concentrations are expected to have an even more significant impact on the ferroelectric properties.

In presenting our results, we non-dimensionalize the coercive field with the classical value $E_{cl}$, which is defined to be the slope of $W_p(p)$ at the spinodal points $\pm p_s$,

$$E_{cl} = \left| \frac{\partial W_p(\pm p_s)}{\partial p} \right|, \ \text{ where } \ \frac{\partial^2 W_p(\pm p_s)}{\partial p^2} = 0. \tag{26}$$

Additionally, we non-dimensionalize the charge density $\rho_0 = \rho/(qN_d)$, the frequency of applied voltage $f_0 = f/\alpha$, and the position $(x)$ by the thickness of the ferroelectric $(L)$. Finally, we use the volume-averaged polarization for plotting the hysteresis loops.

### A. Steady-state profiles

We begin by studying steady-state solutions of the system with no external field. These are shown in Fig. 3. We have verified that these profiles agree with the equilibrium profiles of Xiao et al.[23,25] We briefly describe them, since some of their salient features are useful in understanding subsequent results.

On shorting the circuit, we obtain $\mu_{n_c} = \mu_{N_d^0} - \mu_{N_d^+} = -\mu_{p_v} = -\Phi$. Thus, in the absence of external potential, the entire system equilibrates to a common Fermi level equal to the Fermi energy of the metal.[30] This, in turn, results in the formation of depletion layers near the metal-ferroelectric

TABLE I. List of constants and material parameters.

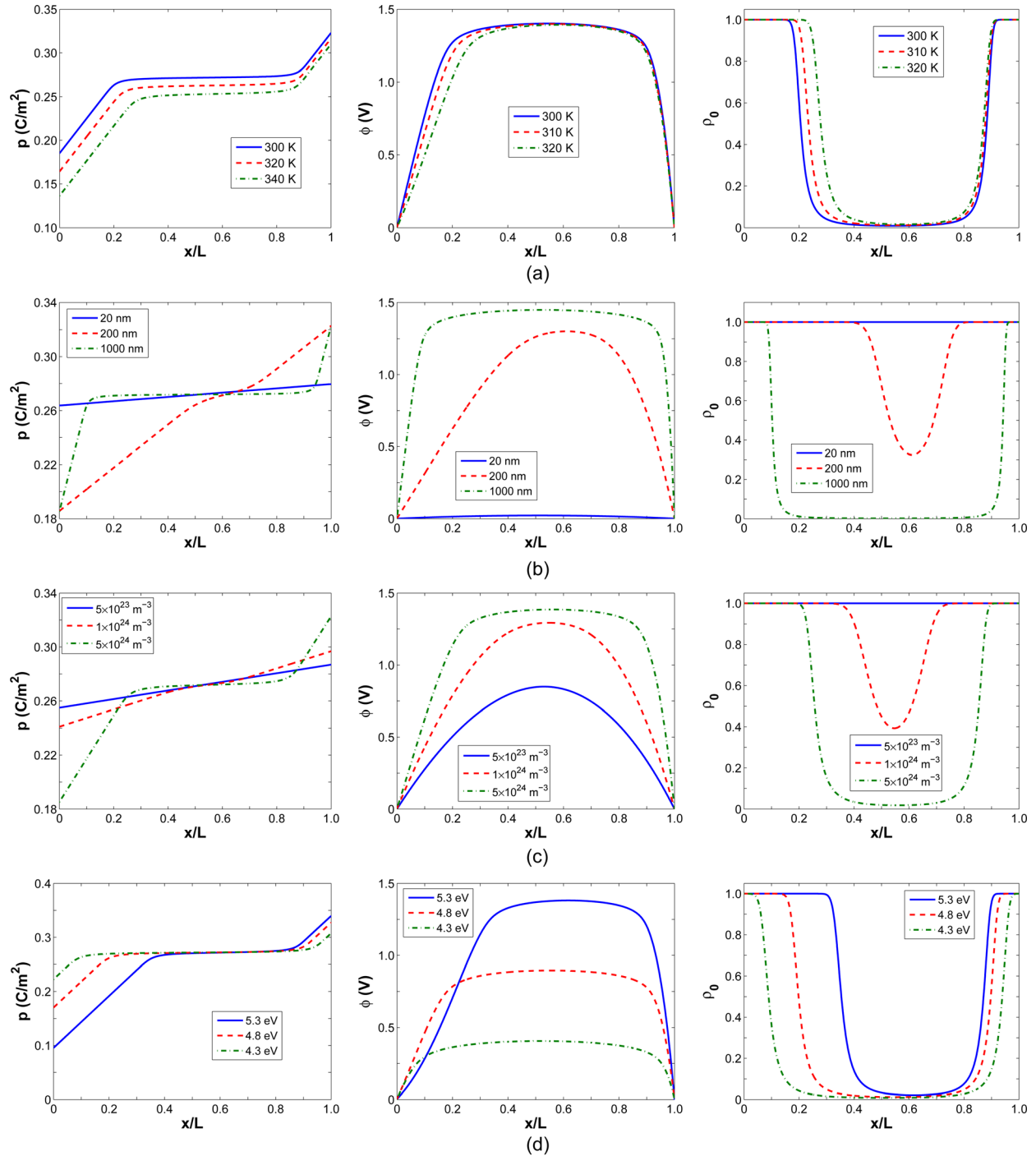| Constant | Value | Constant | Value |
|---|---|---|---|
| $k$ (Vm$^3$C$^{-1}$) | $10^{-9}$ | $a$ (JmC$^{-2}$K$^{-1}$) | $3.3254 \times 10^5$ |
| $T_1$ (K) | 448 | $c$ (Jm$^9$C$^{-6}$) | $6.5332 \times 10^9$ |
| $T_0$ (K) | 383 | $b_0$ (Jm$^5$C$^{-4}$K$^{-1}$) | $3.6347 \times 10^6$ |
| $T$ (K) | 300 | $E_c$ (eV) | $-3.6$ |
| $E_d$ (eV) | $-4.0$ | $E_v$ (eV) | $-6.6$ |
| $P$ (m$^{-3}$) | $10^{24}$ | $N$ (m$^{-3}$) | $10^{24}$ |
| $K_1$ ((eV)$^{-1}$m$^{-1}$s$^{-1}$) | $10^{13} \alpha$ | $K_2$((eV)$^{-1}$m$^{-1}$s$^{-1}$) | $10^{11} \alpha$ |
| $k_1$ (s$^{-1}$) | $10^{11} \alpha$ | $k_2$ (s$^{-1}$) | $10^8 \alpha$ |
| $k_3$ (s$^{-1}$) | $10^8 \alpha$ | $k_4 = k_5$ (m$^{-2}$s$^{-1}$) | $10^{24} \alpha$ |
| $K_3$ | 0 | $K_4$ | 0 |

FIG. 3. (Color online) Steady state profiles of polarization, electrostatic potential, and charge density and its variation with various parameters.

interfaces $S_1$ and $S_2$,[23] whose widths are determined by the electrode work function, ambient temperature, thickness, and doping of the ferroelectric. At low thicknesses and doping, the ferroelectric is completely depleted. Distinct depletion layers appear on increasing either the thickness or the doping. Simultaneously, there is an increase in the built-in potential, saturating at the value corresponding to the magnitude of the difference between the work function of the metal and the ferroelectric. In the depleted region of the ferroelectric, there is a linear increase in the polarization, whereas it is nearly constant in the non-depleted region. Consequently,

depending on the direction of the polarization, the region near either $S_1$ or $S_2$ is a possible site of nucleation for switching, as we confirm below.

## B. Hysteresis loops

A typical hysteresis loop is shown in Fig. 4. We present the polarization versus electric field hysteresis loops for a wide range of situations in Fig. 5. In each of these simulations, we start with a uniform state, ground electrode $C_1$, and apply a sinusoidal voltage to electrode $C_2$. We choose $f_0 = 0.001$ Hz

for obtaining Figs. 5(a)-5(d), thereby limiting the effect of the frequency of loading on the response of the ferroelectric. The results show the polarization versus electric field hysteresis loops for one cycle after the transients settle down in a few cycles.

The evolution of polarization, electrostatic potential, and charge density through one complete cycle is shown in Fig. 4. Let us begin at the point marked A in the figure with zero applied field and positive polarization. The polarization distribution shown on the top left resembles the equilibrium distribution with depletion layers near the metal-ferroelectric interfaces $S_1$ and $S_2$. As we apply a negative electric field, the depletion layer near $S_1$ grows, accompanied by polarization reduction. At point B, a substantial part of the ferroelectric has polarization below the spinodal value (i.e., the unstable regime), and the overall positive distribution becomes unstable. A nucleus of opposite polarization appears, which rapidly grows through the film, resulting in polarization switching and taking us to point C (polarization profile at bottom left). At C, the polarization profile resembles the equilibrium profile. There is no appreciable change

as the field troughs to D and returns to E. Now, as we apply a positive electric field, the depletion layer near $S_2$ grows, becomes unstable at F, and switches to G. This remains stable as the field peaks at H and returns to zero at A.

## C. Effect of thickness and doping

The hysteresis loops for various thicknesses and doping are shown in Figs. 5(a) and 5(b), respectively. We see that the coercive field decreases with increasing thickness and increasing doping. This is shown in greater detail in Figs. 6(a) and 6(b).

We observe that the coercive field is close to the ideal coercive field (corresponding to the spinodal in the energy) for very small thickness and for very small doping levels. This is because the film is completely depleted (Fig. 3) and the polarization is close to uniform. Thus, there is a substantial nucleation barrier, and switching does not occur until the system becomes globally unstable. As either the thickness or the doping levels increase, we see the appearance of depletion layers, accompanied by inhomogeneous polarization
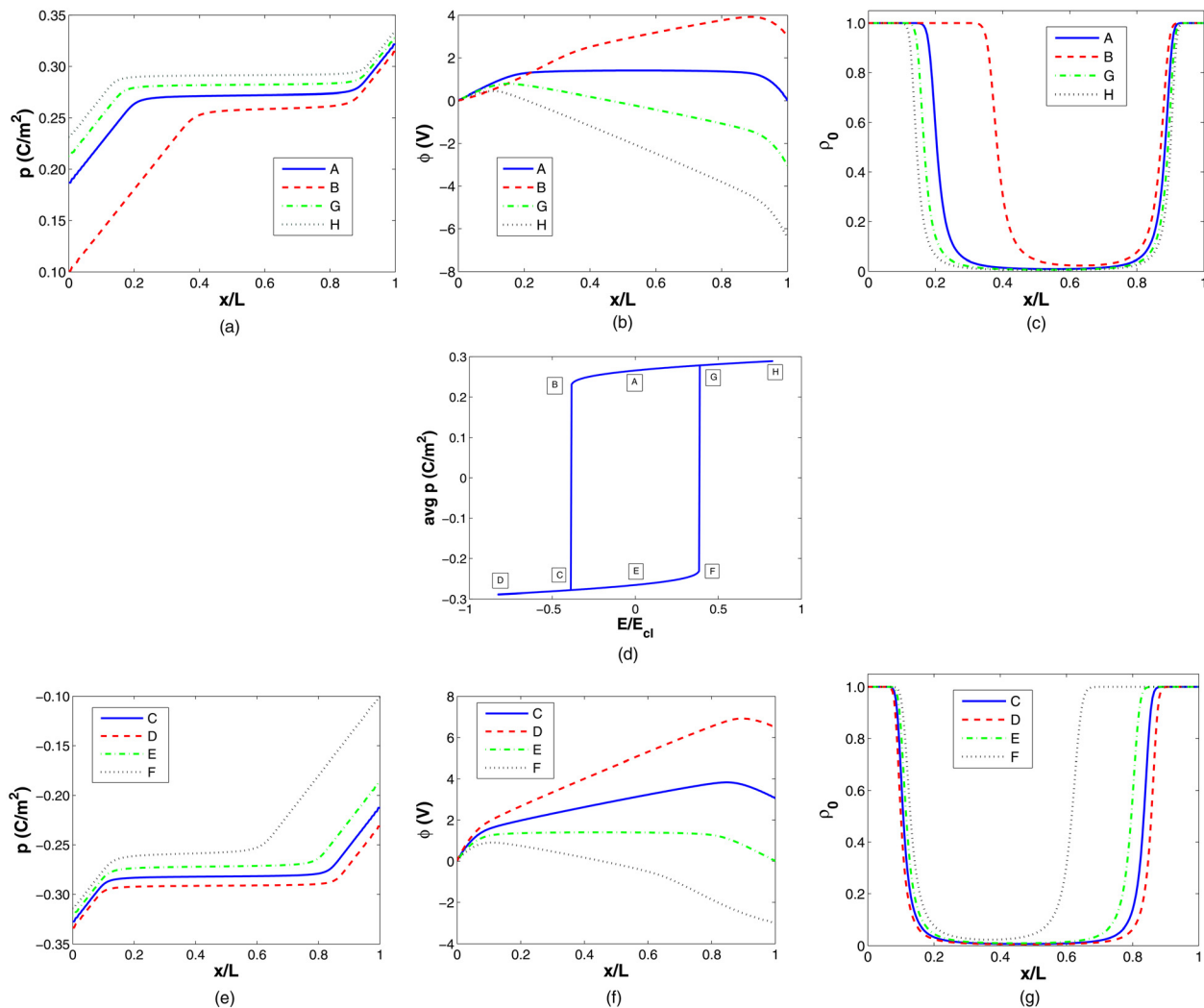


FIG. 4. (Color online) Evolution of polarization, electrostatic potential, and charge density through one complete cycle: $N_d = 5 \times 10^{24}$ m$^{-3}$; $L = 500$ nm; and $f_0 = 0.001$ Hz.

distribution. In particular, we see in Fig. 3 that there is a significant drop of polarization near the electrode.

Consequently, the polarization in this region reaches the spinodal value, even though it is well away from the spinodal in most of the film, resulting in polarization switching at a lower strength of the electric field. Labels A and C in Figs. 6(a) and 6(b) correspond to points after which the film is no longer completely depleted just prior to switching. The coercive field drops dramatically at this point to the bulk value. Further increase of thickness does not decrease the coercive value, consistent with the prior arguments.[4] Indeed, we see in Fig. 3(b) that the polarization profile settles down as the built-in potential saturates at this point. Points B and D in Fig. 6(a) correspond to the thicknesses beyond which the ferroelectric can be considered to have bulk material behavior for the given doping. The results shown here are in agreement with previous theoretical predictions[22,26,28,29,33] as well as experimental observations.[1,34–37]

### D. Effect of work function of metal electrodes

We now examine the impact of the work function of the metal electrodes on the response of the ferroelectric. Figure 6(c) shows the variation of coercive field with the work function of the electrodes. At low values of doping, the work function does not impact the coercive field, but as the doping is increased, there is a pronounced decrease in the coercive electric field with increasing work function. This is a consequence of the diminished polarization values (Fig. 3(d)).

Next, we let the electrodes have different work functions $\Phi_1 \neq \Phi_2$. We observe that the resulting hysteresis loop is not symmetric (Fig. 5(c)). Specifically, $\Phi_1 < \Phi_2$ results in a larger negative coercive field compared to the positive coercive field and vice versa when $\Phi_1 > \Phi_2$. These observations are consistent with experimental observations,[38–40] including those by Feng et al.,[41] who studied the hysteresis loops of

P(VDF-TrFE) thin films with the following metal electrode configurations: Al/Al, Al/Ni, Ni/Al, and Ni/Ni.

### E. Effect of ambient temperature

The variation of the hysteresis loops for different ambient temperatures can be seen in Fig. 5(d), which shows a decrease in the values of the remanent polarization and coercive electric field on increasing the temperature. This is a consequence of the temperature dependence of the Devonshire energy, wherein there is a reduction in the barrier for switching with increasing temperature. The predicted trend is consistent with experimental observations,[42,43] including experiments on thin films of barium titanate in a MFM configuration,[44] where a continuous decrease in the coercive field with increasing temperature was observed.

### F. Effect of frequency of loading

Figures 5(e) and 6(d) show that, on increasing the frequency, the coercive electric field increases, with no apparent change in the remanent polarization. This is in agreement with previously reported experimental observations[45–49] and theoretical predictions.[26,28,29] Further, at low frequencies, the coercive field asymptotes to the quasi-static value, after which there is a transition region over which there is a steady increase in the coercive field until it asymptotes to the classical value of the coercive field ($E_{cl}$) at high frequencies. The frequency dependence of the coercive field is a consequence of the evolution dynamics of the space-charges, which, in turn, affects the profiles of electrostatic potential and polarization. It is worth noting that this is in contrast with previous theoretical models,[26,28,29] where the time dependence was introduced through the Landau-Khalatnikov equation and not the dynamics of the space-charges. In our simulations, as mentioned previously, the time dependence in the Landau-
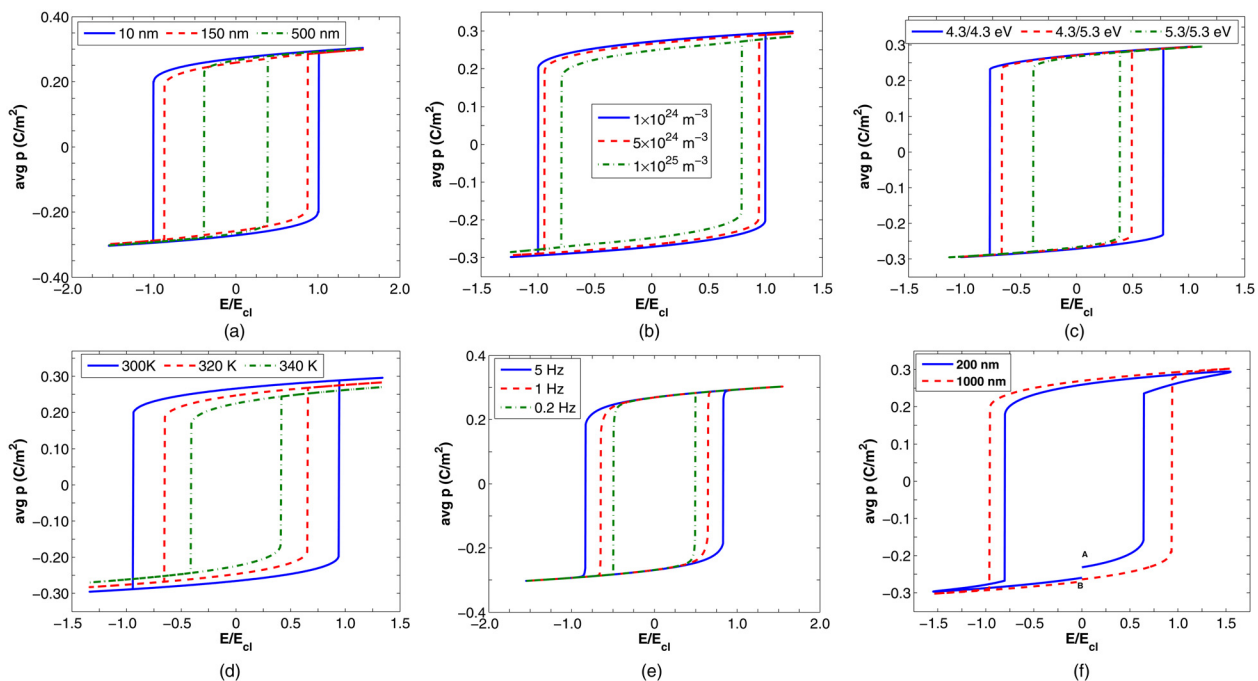


FIG. 5. (Color online) The hysteresis loops under cycling applied voltage and its variation with various parameters.
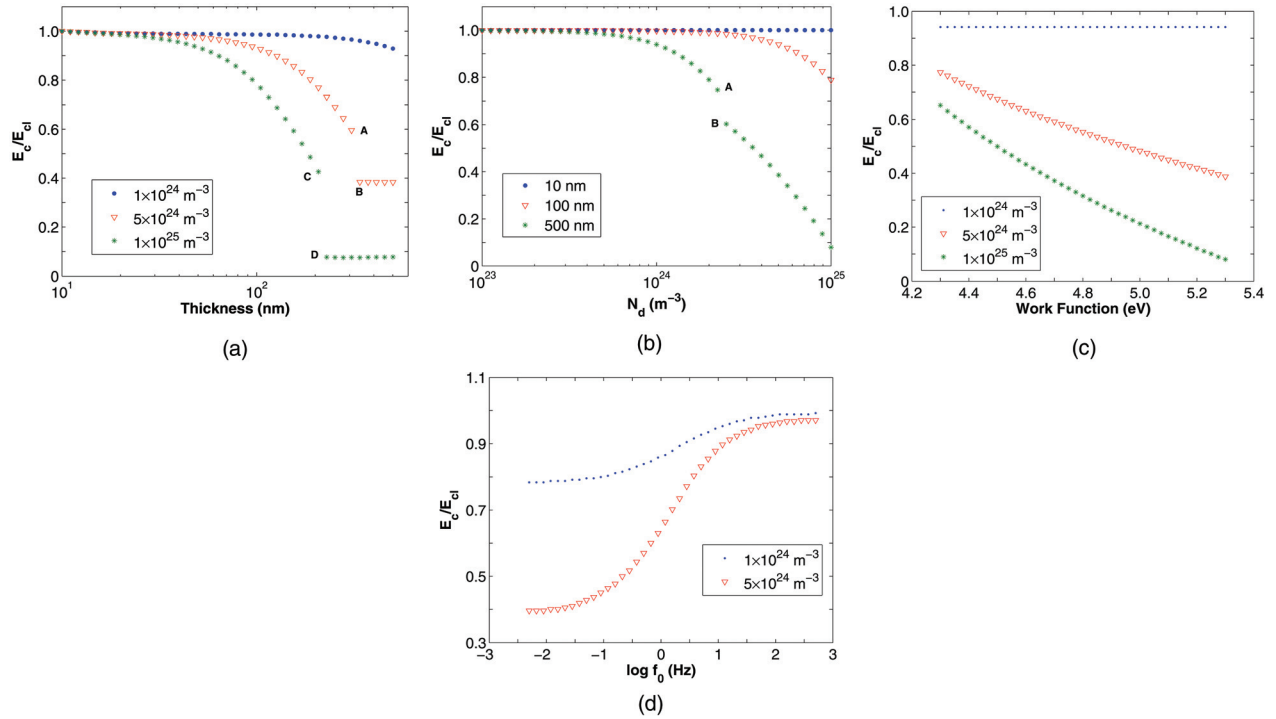
FIG. 6. (Color online) Variation of coercive electric field for different test cases.
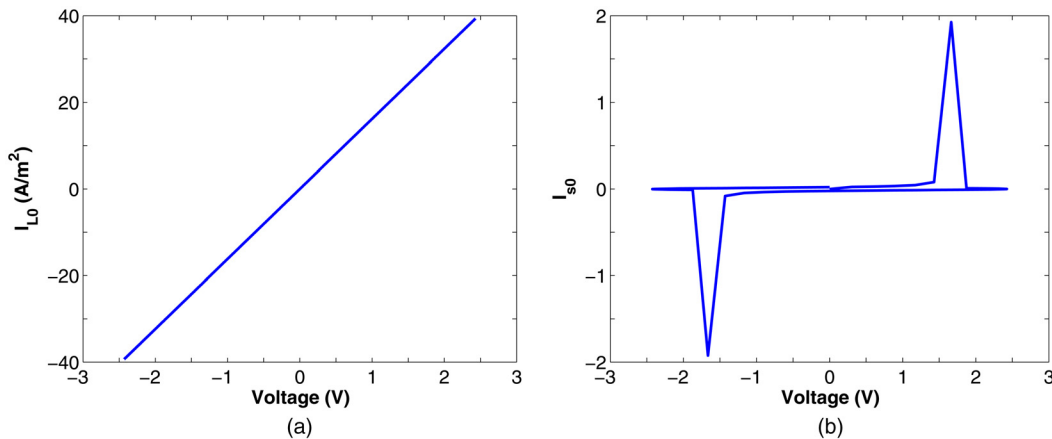
Khalatnikov equation has been set to zero ($\eta = 0$). Therefore, even though the results bear qualitative resemblance, the physical mechanisms are different. For any given situation, the time scales of these phenomena would determine the more appropriate approximation.

## G. Leakage and switching current

The leakage current is evaluated by calculating the flux of electrons through the metal-ferroelectric interface. We obtain a linear relationship between the leakage current and applied voltage, as shown in Fig. 7(a), consistent with some experimental observations,[50,51] where the current-voltage characteristics of a MFM junction with barium titanate as the ferroelectric is found to have a linear relationship at room temperature. In the figure $I_{L0} = \frac{I_L}{A\alpha}$, where $I_L$ is the leakage current and $A$ is the area of the capacitor. However, these

results are in contrast to a number of other experimental studies, which report nonlinear current-voltage behavior.[38,52] In our model, the current-voltage behavior is governed by Eq. (24), which is nonlinear in the voltage. Therefore, one would expect our model to display nonlinear current-voltage characteristics. However, in our simulations, we have obtained results which are close to the solutions of the linearized counterpart of Eqs. (23) and (24). Therefore, in situations where Eq. (23) is far from equilibrium, we expect the model to display nonlinear current-voltage behavior. The exact situations in which such behavior is achieved warrants further investigation. Additionally, we need to ascertain the impact of surface states (neglected in this work) and polydomains on the current-voltage characteristics to achieve a more comprehensive picture.

The charge density on the metal electrodes $\sigma = [|-\varepsilon_0 \frac{\partial \phi}{\partial x} + p|]$ is used to calculate the switching current



FIG. 7. (Color online) Predicted leakage and switching current as a function of applied voltage for $N_d = 5 \times 10^{24}$ m$^{-3}$ and $L = 100$ nm.

shown in Fig. 7(b). The brackets $[|\cdot|]$ denote the jump in a quantity across the interface. $I_{s0} = \frac{I_s}{I_s^0}$, where $I_s$ is the switching current and $I_s^0$ is a normalizing constant. The two peaks correspond to the points at which there is polarization reversal, i.e., when switching occurs. The trend is consistent with previous observations.[47,53,54] It should be noted that, in these simulations, the rate of switching cannot be captured, because we have taken the inverse mobility $\eta = 0$. Therefore, the magnitude of switching current is unrealistic, but its qualitative nature is indeed accurate.

### H. Lossy ferroelectric

Here, we look to capture the lossy nature of the ferroelectric and study its dependence on the thickness and doping of the ferroelectric as well as the frequency of loading. Figure 5(f) shows the hysteresis loops for films of thickness $L = 200$ nm and 1000 nm at $f_0 = 100$ Hz and $N_d = 10^{25}$ m$^{-3}$. We see that the hysteresis loops do not close after one complete cycle, a commonly observed feature in experiments.[55,56] The reason for the gap can be understood by looking at Fig. 8, where the magnitude of net charge in the ferroelectric and on the metal electrodes reduces over one complete cycle. This is due to the fact that, at high frequencies of loading, the space charges do not get sufficient time to equilibrate, i.e., the relaxation time of the space charges is significantly larger than the time period of loading. This gap is found to reduce on increasing the thickness, which is consistent with previous observations,[57] where thin films are found to be an order of magnitude more lossy than their bulk counterparts. We also observe an increase in the size of the gap on increasing the doping level and the frequency of loading. In contrast, for the quasi-static calculations, the ferroelectric does not lose any charge and, hence, the hysteresis loop is always closed. Similar conclusions have been reported in the literature,[58] where the effects of the leakage current and frequency of loading on the hysteresis loop gap were studied for a PZT capacitor with Pt electrodes. Interestingly, the non-closure of hysteresis loops observed experimentally is a consequence of leakage currents, which are usually asymmetric with respect to the applied bias. Further, leakage-induced contributions to the hysteresis loop are larger at lower frequencies, clearly distinguishing itself from the results presented here. Another interesting aspect to note is the asymmet-
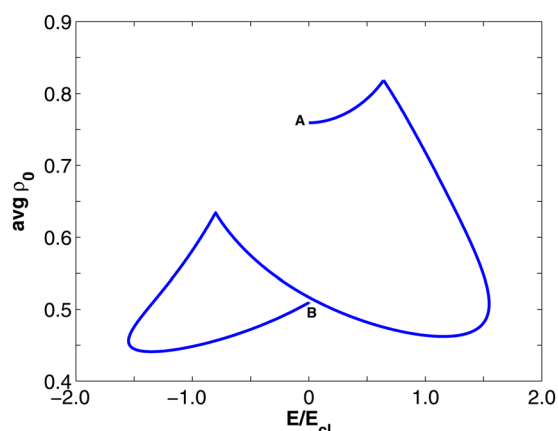
ric nature of the hysteresis loop for the 200-nm-thick film. It shows that, other than having metal electrodes with different work functions, sometimes a high frequency of loading can also result in asymmetric hysteresis loops.

## IV. CONCLUSIONS

We have developed a time-dependent, thermodynamically consistent, continuum formulation for semiconducting ferroelectrics. Specifically, we have developed thermodynamically consistent kinetic equations, which describe the evolution of polarization and space charges when subjected to a time-varying applied field. Moreover, we have systematically included band-bending and other subtle effects resulting from the presence of metal-ferroelectric interfaces. We have used the model to highlight the pronounced effect of the semiconducting nature of ferroelectrics on domain switching, hysteresis, and leakage currents. Further, we have studied how hysteresis and leakage are affected by doping, film thickness, electrode work function, ambient temperature, and loading frequency. All the predictions made by the model are in very good agreement with experimental observations and previous studies, highlighting the efficacy of the model. The limitation of the model is the presence of constants whose precise values are not known at this point in time. Another limitation of the present work is that the simulations have been restricted to one-dimensional through the thickness calculations. This has limited the situations encountered to mono-domain states rather than the typically observed polydomain states with domain walls. We would expect that, in particular, the closure domains near the surface of the ferroelectric have a non-trivial interaction with the depletion layers. This necessitates accurate three-dimensional simulations, which will further shed light on the response/behavior of ferroelectrics. This is a subject of future investigation by the authors.

We believe that the proposed model is an important step toward being able to characterize ferroelectric devices, particularly those utilizing thin films. We are currently using ideas developed in this work to understand how illumination of light can be used for domain patterning, a subject of great technological interest. We also expect such a model to be useful in understanding the mechanisms involved in the fracture of ferroelectrics, which is currently an open problem and being pursued by the authors.

## APPENDIX A: RATE OF DISSIPATION OF SYSTEM

In this appendix, we show that the proposed model is thermodynamically consistent. Specifically, we verify that it satisfies the second law of thermodynamics. In the current setting of isothermal processes, this is equivalent to showing that the rate of dissipation is positive in any allowable process.

We also note that the presentation below offers an alternate route for deriving the equations. In the development in Sec. II, we used first variations of the potential energy to



FIG. 8. (Color online) Average charge density through one complete cycle for L $= 200$ nm, $N_d = 10^{25}$ m$^{-3}$, and $f_0 = 100$ Hz.

identify the chemical potentials and the driving force. An alternate approach follows Coleman and Noll,[59] where these quantities, as well as their dependence on kinematic quantities, are identified using the dissipation inequality and the requirement that this inequality be satisfied by all processes.

### 1. Rate of dissipation

The rate of dissipation $\mathcal{D}$ of the entire system can be expressed in terms of the rate of external working $\mathcal{F}$ and the rate of the change of the total energy $\frac{d\mathcal{E}}{dt}$,

$$\mathcal{D} = \mathcal{F} - \frac{d\mathcal{E}}{dt}. \tag{A1}$$

### 2. Rate of external working

$$\mathcal{F} = \frac{d}{dt}\int_{C_2} V\sigma\,\mathrm{d}S - \int_{\partial\Omega}\mu_{n_c}\mathbf{J_{n_c}}\cdot\hat{\mathbf{m}}\,\mathrm{d}S - \int_{\partial\Omega}\mu_{p_v}\mathbf{J_{p_v}}\cdot\hat{\mathbf{m}}\,\mathrm{d}S$$
$$- \int_{\partial\Omega}\mu_{N_d^0}\mathbf{J_{N_d^0}}\cdot\hat{\mathbf{m}}\,\mathrm{d}S - \int_{\partial\Omega}\mu_{N_d^+}\mathbf{J_{N_d^+}}\cdot\hat{\mathbf{m}}\,\mathrm{d}S. \tag{A2}$$

Here, $\mu$ refers to the chemical potential of the respective subscripted quantity, and $\sigma$ is the charge density on $C_2$. The first term in Eq. (A2) evaluates the rate of work done by the battery, and the remaining terms represent the chemical energy due to the flux of the respective quantities. Using the divergence theorem and Eq. (4), it follows

$$\mathcal{F} = \frac{d}{dt}\int_{C_2} V\sigma\,\mathrm{d}S - \int_{\Omega}\left(\nabla\mu_{n_c}\cdot\mathbf{J_{n_c}} + \nabla\mu_{p_v}\cdot\mathbf{J_{p_v}} + \nabla\mu_{N_d^0}\cdot\mathbf{J_{N_d^0}}\right.$$
$$+ \nabla\mu_{N_d^+}\cdot\mathbf{J_{N_d^+}}\right)\mathrm{d}x + \int_{\Omega}\left(\mu_{n_c}\dot{n}_c + \mu_{p_v}\dot{p}_v + \mu_{N_d^0}\dot{N}_d^0\right.$$
$$\left.+ \mu_{N_d^+}\dot{N}_d^+\right)\mathrm{d}x - \int_{\Omega}(\mu_{n_c} + \mu_{N_d^+} - \mu_{N_d^0})\xi_{cd}\,\mathrm{d}x$$
$$- \int_{\Omega}(\mu_{n_c} + \mu_{p_v})\xi_{cv}\,\mathrm{d}x - \int_{\Omega}(\mu_{p_v} + \mu_{N_d^0} - \mu_{N_d^+})\xi_{dv}\,\mathrm{d}x. \tag{A3}$$

### 3. Rate of change of total energy

The total energy of the system, $\mathcal{E}$, comprised of the energy stored in the ferroelectric $W$ and the energy due to the electrostatic potential in all of space. Therefore,

$$\frac{d\mathcal{E}}{dt} = \int_{\Omega}\dot{W}\mathrm{d}x + \frac{d}{dt}\left(\frac{1}{2}\int_{\mathbb{R}^3}\varepsilon_0|\nabla\phi|^2\mathrm{d}x\right). \tag{A4}$$

At this point, we make the constitutive assumption $W = W(\mathbf{p}, \nabla\mathbf{p}, n_c, p_v, N_d^0, N_d^+)$. On using the chain rule and divergence theorem,

$$\int_{\Omega}\dot{W}\mathrm{d}x = \int_{\Omega}\left(\frac{\partial W}{\partial n_c}\dot{n}_c + \frac{\partial W}{\partial p_v}\dot{p}_v + \frac{\partial W}{\partial N_d^0}\dot{N}_d^0 + \frac{\partial W}{\partial N_d^+}\dot{N}_d^+\right)\mathrm{d}x$$
$$+ \int_{\Omega}\left(\frac{\partial W}{\partial\mathbf{p}}\cdot\dot{\mathbf{p}} - \left(\nabla\cdot\frac{\partial W}{\partial\nabla\mathbf{p}}\right)\cdot\dot{\mathbf{p}}\right)\mathrm{d}x$$
$$+ \int_{\partial\Omega}\left(\frac{\partial W}{\partial\nabla\mathbf{p}}\hat{\mathbf{m}}\right)\cdot\dot{\mathbf{p}}\,\mathrm{d}S. \tag{A5}$$

Also, it can be shown that[24]

$$\frac{d}{dt}\left(\frac{1}{2}\int_{\mathbb{R}^3}\varepsilon_0|\nabla\phi|^2\mathrm{d}x\right) = \int_{\Omega}\nabla\phi\cdot\dot{\mathbf{p}}\,\mathrm{d}x + \int_{\Omega}\phi\dot{\rho}\,\mathrm{d}x$$
$$+ \frac{d}{dt}\int_{C_2}V\sigma\,\mathrm{d}S. \tag{A6}$$

### 4. Expression for rate of dissipation

Using Eqs. (3), (A1), (A3)–(A5) and (A6) we obtain the following expression for the rate of dissipation of the system:

$$\mathcal{D} = -\int_{\Omega}\left(\nabla\mu_{n_c}\cdot\mathbf{J_{n_c}} + \nabla\mu_{p_v}\cdot\mathbf{J_{p_v}} + \nabla\mu_{N_d^0}\cdot\mathbf{J_{N_d^0}}\right.$$
$$\left.+ \nabla\mu_{N_d^+}\cdot\mathbf{J_{N_d^+}}\right)\mathrm{d}x - \int_{\Omega}(\mu_{n_c} + \mu_{N_d^+} - \mu_{N_d^0})\xi_{cd}\,\mathrm{d}x$$
$$- \int_{\Omega}(\mu_{n_c} + \mu_{p_v})\xi_{cv}\,\mathrm{d}x - \int_{\Omega}(\mu_{p_v} + \mu_{N_d^0} - \mu_{N_d^+})\xi_{dv}\,\mathrm{d}x$$
$$+ \int_{\Omega}\left(\mu_{n_c} - \frac{\partial W}{\partial n_c} + q\phi\right)\dot{n}_c\,\mathrm{d}x + \int_{\Omega}\left(\mu_{p_v} - \frac{\partial W}{\partial p_v} - q\phi\right)\dot{p}_v\,\mathrm{d}x$$
$$+ \int_{\Omega}\left(\mu_{N_d^0} - \frac{\partial W}{\partial N_d^0}\right)\dot{N}_d^0\,\mathrm{d}x + \int_{\Omega}\left(\mu_{N_d^+} - \frac{\partial W}{\partial N_d^+} - q\phi\right)\dot{N}_d^+\,\mathrm{d}x$$
$$+ \int_{\Omega}\left(\nabla\cdot\left(\frac{\partial W}{\partial\nabla\mathbf{p}}\right) - \frac{\partial W}{\partial\mathbf{p}} - \nabla\phi\right)\cdot\dot{\mathbf{p}}\,\mathrm{d}x - \int_{\partial\Omega}\left(\frac{\partial W}{\partial\nabla\mathbf{p}}\hat{\mathbf{m}}\right)\cdot\dot{\mathbf{p}}\,\mathrm{d}S. \tag{A7}$$

Notice that each of these terms is a product of a flux (or rate or generalized velocity) and a gradient (or potential or driving force). Further, we can substitute the relations in Sec. II to verify that each of these terms is non-negative. Thus, the rate of dissipation is non-negative, and the model is thermodynamically consistent.

[1] F. Jona and G. Shirane, *Ferroelectric Crystals*, International Series of Monographs on Solid State Physics (Pergamon, New York, 1962), Vol. 1.
[2] P. Muralt, J. Micromech. Microeng. **10**(11), 136 (2000).
[3] K. Buse, A. Adibi, and D. Psaltis, Nature **393**, 665 (1998).
[4] D. Damjanovic, Rep. Prog. Phys. **61**(9), 1267 (1998).
[5] J. F. Scott, K. Watanabe, A. J. Hartmann, and R. N. Lamb, Ferroelectrics **225**, 83 (1999).
[6] A. J. Moulson and K. H. Herbert, *Electroceramics: Materials, Properties, Applications* (Wiley, New York, 2003).
[7] A. F. Devonshire, Philos. Mag. **40**(309), 1040 (1949).
[8] A. F. Devonshire, Philos. Mag. **42**(333), 1040 (1949).
[9] K. Bhattacharya and G. Ravichandran, Acta Mater. **51**(19), 5941 (2003).
[10] C. Dearaujo, J. D. Cuchiaro, L. D. McMillan, M. C. Scott, and J. F. Scott, Nature **374**(6523), 627 (1995).
[11] R. Ramesh, W. K. Chan, B. Wilkens, H. Gilchrist, T. Sands, J. M. Tarascon, V. G. Keramidas, D. K. Fork, J. Lee, and A. Safari, Appl. Phys. Lett. **61**(13), 1537 (1992).
[12] J. F. Scott and C. A. Paz de Araujo, Science **246**(4936), 1400 (1989).
[13] M. Calleja, M. T. Dove, and E. K. H. Salje, J. Phys.: Condens. Matter **15**, 2301 (2003).
[14] D. Shilo, G. Ravichandran, and K. Bhattacharya, Nature Mater. **3**(7), 453 (2004).
[15] Y. Watanabe, Appl. Surf. Sci. **130–132**, 610 (1998).
[16] Y. Watanabe, Phys. Rev. B **57**(2), 789 (1998).
[17] Y. Watanabe, J. Appl. Phys. **83**(4), 2179 (1998).
[18] Y. Watanabe and D. Sawamura, Jpn. J. Appl. Phys. **36**(9B), 6162 (1997).
[19] L. Pintilie and M. Alexe, J. Appl. Phys. **98**(12), 124103 (2005).
[20] A. M. Bratkovsky and A. P. Levanyuk, AIP Conf. Proc. **535**, 229 (2000).
[21] A. K. Tagantsev, C. Z. Pawlaczyk, K. Brooks, M. Landivar, E. Colla, and N. Setter, Integr. Ferroelectr. **6**, 309 (1995).

[22]P. Zubko, D. J. Jung, and J. F. Scott, J. Appl. Phys. **100**(11), 114112 (2006).

[23]Y. Xiao, V. B. Shenoy, and K. Bhattacharya, Phys. Rev. Lett. **95**(24), 247603 (2005).

[24]Y. Xiao and K. Bhattacharya, Arch. Ration. Mech. Anal. **189**(1), 59 (2008).

[25]V. B. Shenoy, Y. Xiao, and K. Bhattacharya, "Effect of doping on polarization profiles and switching in ferroelectric thin films," J. Appl. Phys. (submitted).

[26]A. N. Morozovska and E. A. Eliseev, J. Phys.: Condens. Matter **16**(49), 8937 (2004).

[27]A. N. Morozovska, Ferroelectrics **317**, 229 (2005); paper presented at the NATO Advanced Research Workshop on Dimensionality Effects and Nonlinearity in Ferroics, Lviv, Ukraine, 19–22 October 2004.

[28]A. N. Morozovska and E. A. Eliseev, Physica B **355**(1–4), 236 (2005).

[29]A. N. Morozovska and E. A. Eliseev, Phys. Status Solidi B **242**(4), 947 (2005).

[30]S. Sze, *Physics of Semiconductor Devices* (Wiley-Interscience, New York, 1981).

[31]R. Enderlein and N. J. M. Horing, *Fundamentals of Semiconductor Physics and Devices* (World Scientific, Singapore, 1997).

[32]P. Rabinowitz, *Numerical Methods for Nonlinear Algebraic Equations* (Gordon and Breach, New York, 1970).

[33]L. Baudry and J. Tournier, J. Appl. Phys. **97**(2), 024104 (2005).

[34]J. Rodríguez Contreras, H. Kohlstedt, U. Poppe, R. Waser, C. Buchal, and N. A. Pertsev, Appl. Phys. Lett. **83**(22), 4595 (2003).

[35]N. A. Pertsev, J. Rodríguez Contreras, V. G. Kukhar, B. Hermanns, H. Kohlstedt, and R. Waser, Appl. Phys. Lett. **83**(16), 3356 (2003).

[36]W. Liu, W. Chen, L. Yang, L. Zhang, Y. Wang, C. Zhou, S. Li, and X. Ren, Appl. Phys. Lett. **89**(17), 172908 (2006).

[37]X. Wang and H. Ishiwara, Appl. Phys. Lett. **82**(15), 2479 (2003).

[38]P. W. M. Blom, R. M. Wolf, J. F. M. Cillessen, and M. P. C. M. Krijn, Phys. Rev. Lett. **73**(15), 2107 (1994).

[39]I. Boerasu, L. Pintilie, M. Pereira, M. I. Vasilevskiy, and M. J. M. Gomes, J. Appl. Phys. **93**(8), 4776 (2003).

[40]F. Xia and Q. M. Zhang, Mater. Res. Soc. Symp. Proc. **734**, 261 (2003).

[41]F. Xia and Q. M. Zhang, Appl. Phys. Lett. **85**(10), 1719 (2004).

[42]Y. Akishige, J. Phys. Soc. Jpn. **75**(7), 073704 (2006).

[43]A. S. Sidorkin, L. P. Nesterenko, I. A. Bocharova, G. L. Smirnov, V. A. Sidorkin, and S. V. Ryabtsev, J. Phys. IV **126**, 81 (2005).

[44]H. Basantakumar Sharma and A. Mansingh, J. Phys. D **31**(13), 1527 (1998).

[45]A. Jiang, M. Dawber, J. F. Scott, C. Wang, P. Migliorato, and M. Gregg, Jpn. J. Appl. Phys. **42**(11), 6973 (2003).

[46]O. Lohse, M. Grossmann, U. Boettger, D. Bolten, and R. Waser, J. Appl. Phys. **89**(4), 2332 (2001).

[47]R. Meyer, R. Waser, K. Prume, T. Schmitz, and S. Tiedke, Appl. Phys. Lett. **86**(14), 142907 (2005).

[48]S.-M. Nam, Y.-B. Kil, S. Wada, and T. Tsurumi, Jpn. J. Appl. Phys. **42**, L1519 (2003).

[49]J. Yin and W. Cao, Appl. Phys. Lett. **80**(6), 1043 (2002).

[50]D.-H. Do, "Investigation of ferroelectricity and piezoelectricity in ferroelectric thin film capacitors using synchrotron x ray microdiffraction," Ph.D. dissertation, University of Wisconsin-Madison, 2006.

[51]M. P. Singh, L. Méchin, W. Prellier, and M. Maglione, Appl. Phys. Lett. **89**(20), 202906 (2006).

[52]C. Sudhama, A. C. Campbell, P. D. Maniar, R. E. Jones, R. Moazzami, C. J. Mogab, and J. C. Lee, J. Appl. Phys. **75**(2), 1014 (1994).

[53]R. C. G. Naber, B. de Boer, P. W. M. Blom, and D. M. de Leeuw, Appl. Phys. Lett. **87**(20), 203509 (2005).

[54]D.-Y. Wang and C.-Y. Chang, Jpn. J. Appl. Phys. **44**(4A), 1857 (2005).

[55]R. Thomas, S. Mochizuki, T. Mihara, and T. Ishida, Thin Solid Films **413**, 65 (2002).

[56]S. Yamauchi, H. Tamura, M. Yoshimaru, and M. Ino, Jpn. J. Appl. Phys. **32**, 4118 (1993).

[57]A. K. Tagantsev, V. O. Sherman, K. F. Astafiev, J. Venkatesh, and N. Setter, J. Electroceram. **11**(1-2), 5 (2003).

[58]Z. Lirong, W.-P. Xu, P. Yang, and L. Chenglu, in *9th International Symposium on Electrets, 1996* (ISE 9), Shanghai, China, 25–30 September 1996, pp. 920–924.

[59]R. D. Coleman and W. Noll, Arch. Ration. Mech. Anal. **13**(3), 167 (1963).